LEGIBILITY NOTICE

A major purpose of the Technical Information Center is to provide the broadest dissemination possible of information contained in DOE's Research and Development Reports to business, industry, the academic community, and federal, state and local governments.

Although a small portion of this report is not reproducible, it is being made available to expedite the availability of information on the research discussed herein.

LA-UR--90-2909

DE90 016433

TITLE: NUCLEAR STRUCTURE CALCULATIONS FOR ASTROPHYSICAL APPLICATIONS

AUTHOR(S): Peter Moller, J. Rayford Nix, Karl-Ludwig Kratz, and W. Michael Howard

SUBMITTED TO: Presented at the Internatioanl Symposium on Nuclear Astrophysics: "Nuclei in the Cosmos," Baden/Vienna, Austria, June 18-22, 1990.

NUCLEAR STRUCTURE CALCULATIONS FOR ASTROPHYSICAL APPLICATIONS

P. Möller, J. R. Nix, K.-L. Kratz and W. M. Howard

August 15, 1990

Presented at the International Symposium on Nuclear Astrophysics:
"Nuclei in the Cosmos," Baden/Vienna, Austria, June 18–22, 1990

Preprint LA-UR-90

NUCLEAR STRUCTURE CALCULATIONS FOR ASTROPHYSICAL APPLICATIONS

PETER MÖLLER
Department of Mathematical Physics, Lund Institute of Technology, Box 118, S-22100 Lund, Sweden

J. RAYFORD NIX
Theoretical Division, Los Alamos National Laboratory, Los Alamos, New Mexico 87545, USA

KARL-LUDWIG KRATZ
Johannes Gutenberg Universität, Institut für Kernchemie, Postfach 3980, 6500 Mainz, FRG

W. MICHAEL HOWARD
Lawrence Livermore National Laboratory, L-297, Livermore, California 94550, USA

1. Introduction

Relative to other fields of physics, astrophysics is probably unique in its requirement that a very large number of physical environments be modeled to achieve a satisfactory description of the phenomena under study. The dynamics of the cosmos is governed by interactions that span a vast range, from subnucleon, nucleon and nuclear distances to distances affected by the gravitational interaction, which extends over the width of a galaxy and beyond, to the edge of the universe. It is the nuclear processes that provide much of the energy that drives the macroscopic behaviour of the cosmos. Through this energy release the behaviour on the very small scale is coupled to the very large-scale behaviour.

On the nuclear level, cross sections, nuclear decay energies and nuclear decay paths are but a few examples of quantities that are of paramount importance in astrophysical models. Because nuclei of extreme composition, quite different from what can be studied on earth, exist in stellar environments, an understanding of the nuclear structure properties of these nuclei can only be obtained through theoretical means. This presents a continuing, stimulating challenge to the nuclear-physics community.

Here we present calculated results on such diverse properties as nuclear energy levels, ground-state masses and shapes, β-decay properties and fission-barrier heights. Our approach to these calculations is to use a unified theoretical framework within which the above properties can all be studied. The results are obtained in the macroscopic-microscopic approach [1-3]) in which a microscopic nuclear-structure single-particle model with extensions is combined with a macroscopic model, such as the liquid-drop model. In this model the total potential energy of the nucleus can be calculated as a function

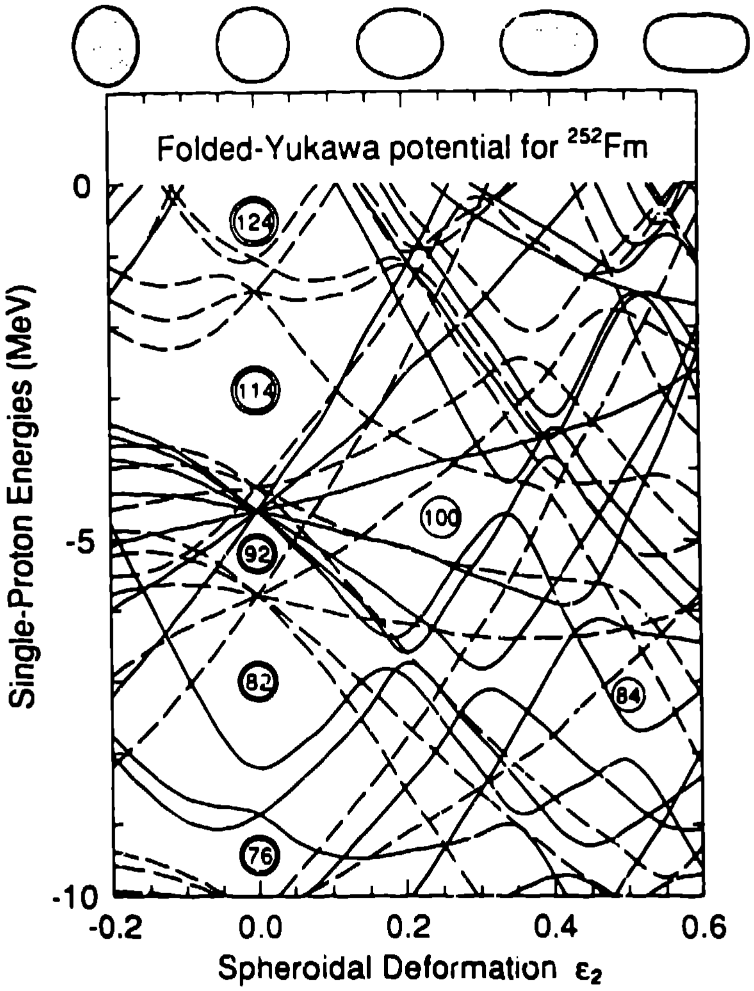

Figure 1: Calculated proton single-particle levels in the ^{252}Fm region. The nuclear shapes, corresponding to those shown at the top of the figure, are labelled by their component of spheroidal deformation ϵ_2. The spherical magic proton numbers 82 and 114 at lead and the superheavy island, respectively, are clearly visible. For deformed shapes the proton number $Z = 100$ corresponds to a particularly stable configuration.

of shape. The maxima and minima in this function correspond to such features as the ground state, fission saddle points and shape-isomeric states. Various transition-rate matrix elements are determined from wave functions calculated in the single-particle model with pairing and other relevant residual interactions taken into account.

2. Calculated results

2.1. SINGLE-PARTICLE MODEL

To illustrate important features of the microscopic model we show in fig. 1 calculated proton single-particle levels for a sequence of shapes leading from slightly oblate shapes to elongated shapes that start to develop an indentation or neck midway between the

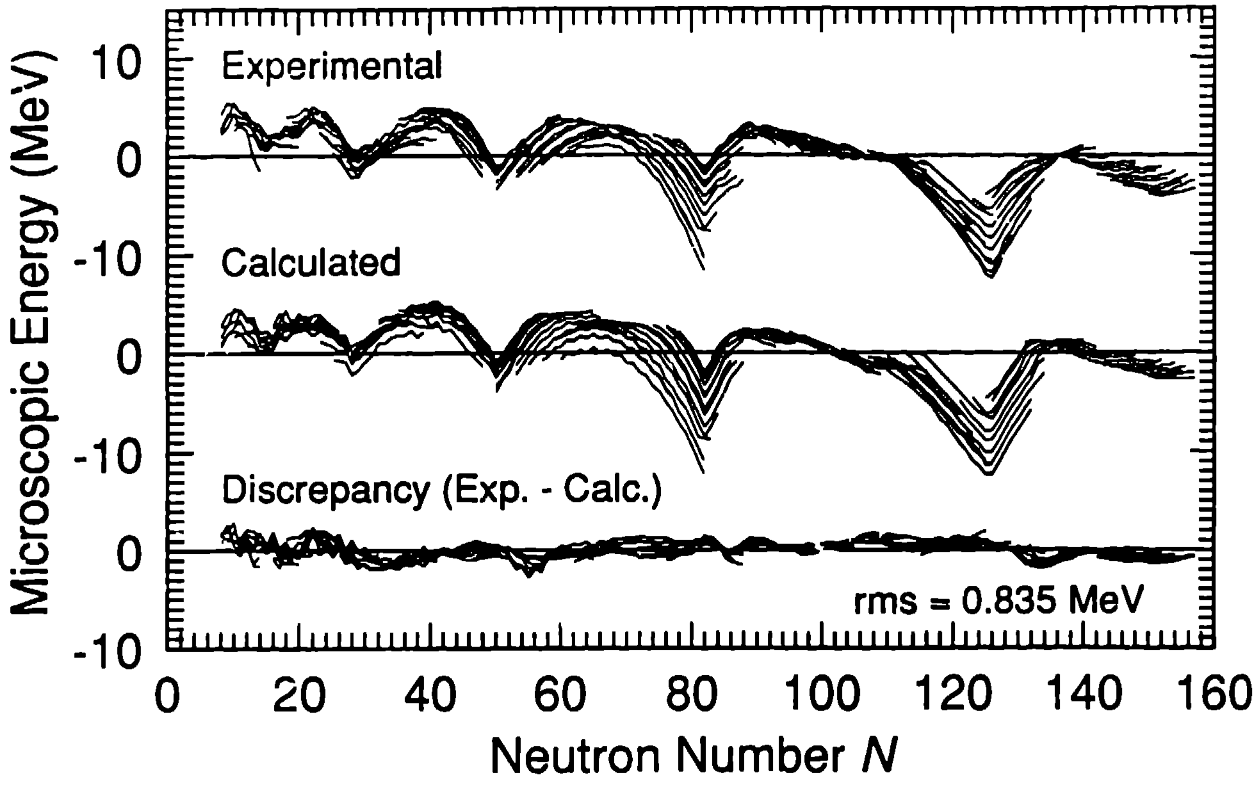

Figure 2: Difference between experimental and calculated ground-state masses (bottom part of figure). The deviations in the vicinity of neutron number $N = 132$ are mostly removed if octupole shape degrees of freedom are considered when the potential energy is minimized.

endpoints. The actual shapes are obtained by rotating the two-dimensional cuts in the top part of the figure about the horizontal symmetry axis. The figure shows several significant features, notably the gaps at the spherical shape and the gap at proton number $Z = 100$ for deformed shapes. For shapes with $\epsilon_2 \leq 0.20$, ϵ_4 is zero; beyond this value ϵ_4 increases linearly to 0.08 at $\epsilon_2 = 0.60$ to allow for a suitable neck formation. The figure indicates that $Z = 114$ is the next magic proton number beyond the gap $Z = 82$ at lead. Gaps in the deformed region such as the $Z = 100$ gap give rise to extra stability at the corresponding shape and counteract the liquid-drop-model driving force towards spherical shapes. The end result is that most nuclei in regions between magic numbers are deformed in their ground state.

2.2. GROUND-STATE MASSES AND MICROSCOPIC CORRECTIONS

To obtain the potential energy of the nucleus at a specific shape the microscopic shell and pairing corrections are determined from the single-particle level spectra for protons and neutrons by use of Strutinsky's method and added to the macroscopic contribution calculated in a liquid-drop model. The minimum as a function of shape of this sum defines the nuclear ground-state mass and corresponding shape coordinates. The difference between the experimental mass and the theoretical mass, as calculated in the macroscopic model only, is defined as the experimental microscopic correction. We show such microscopic corrections in the top part of fig. 2, taken from ref. [4]). The middle part shows microscopic corrections calculated from levels obtained in a folded-Yukawa single-particle potential. Lines connect isotopes of the same element. The bottom part shows the difference between the calculated and experimental microscopic corrections, which is equivalent to the difference between the calculated and experimental ground-state masses.

Rather than embarking on a detailed discussion of the deviations between experimental and theoretical masses we direct the reader to ref. [4]). However, we wish to point out a few important features. First, one should note that the model used in the calculation contains only about 20 parameters, a very limited number [5]) when compared to most other nuclear mass models. Second, in contrast to other mass models in the 1988 compilation [5]), our approach, with the above limited parameter set, can also be used to determine nuclear ground-state shapes, rotational band-head energies and spins, β-decay rates and fission-barrier structure.

Naturally, one wants to obtain as good agreement as possible between calculations based on this model and experimental data. However, it is counterproductive to strive to reach this goal by introducing a multitude of parameters or by using parameter values that lack a sound physical basis. The absence of correlated deviations between experimental data and model results that is often the outcome of such an approach leaves the scientist unable to gain new insight by interpreting such remaining deviations in terms of new physical effects. Figure 2 provides an interesting illustration of this point. In the analysis of the original calculation it was realized that the low-lying negative-parity states in the region around $N = 132$ suggested that the deviations here might be removed if octupole shape degrees of freedom were taken into account. A minimization of the potential energy with respect to this degree of freedom was performed and showed that this interpretation was indeed correct [4]). The octupole degree of freedom almost entirely removed the discrepancy between calculated and experimental masses in the vicinity of ^{222}Ra. This observation provided the seed stimulus for a revived and rapidly growing interest in the properties of nuclei in this region [6]).

The model used in the 1980 mass calculation has been used with some improvements in the pairing model and some other minor modifications to calculate nuclear masses in the region between the proton and neutron drip lines from ^{16}O to $A = 339$. In fig. 3 we show preliminary microscopic corrections obtained in this calculation. The doubly magic regions with their high degree of stability stand out as lighter shaded areas in this figure. Of particular interest is to observe the superheavy region centered at $Z = 114$ and $N = 178$ and the extension of this region towards the last known elements in terms of a peninsula of relatively large microscopic corrections. It is the tip of this peninsula that has been probed through the discoveries at GSI [7,8]) of elements with $Z = 107$, 108 and 109. Some of the most neutron-rich nuclei that are now accessible for study lie in the vicinity of the doubly magic nucleus ^{132}Sn, where, for example, the half-life of the r-process waiting nucleus ^{130}Cd has been determined [9]). Nuclei on the proton drip line are studied over a large area above ^{100}Sn.

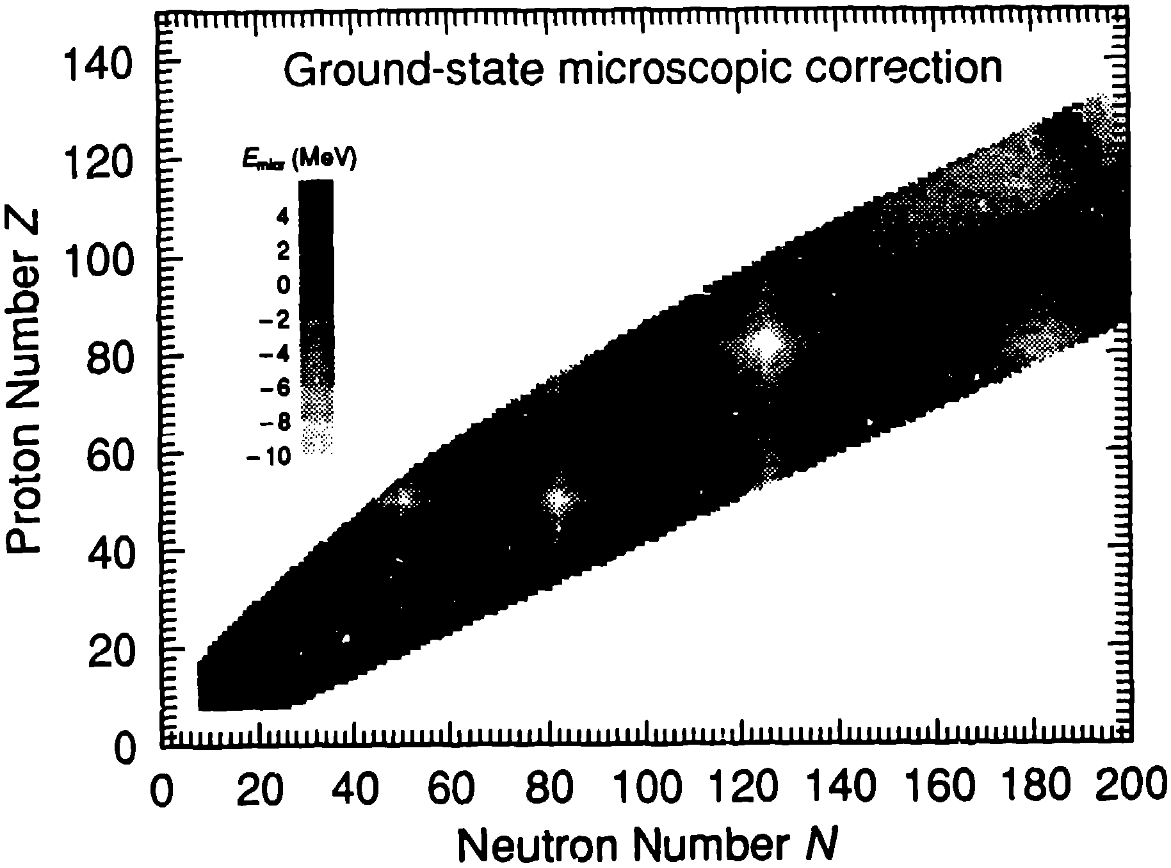

Figure 3: Calculated ground-state microscopic corrections from the proton drip line to the neutron drip line. Lighter shades of gray indicate more stable configurations.

2.3. BETA-DECAY PROPERTIES

The structure observed experimentally in Gamow-Teller β-strength functions very directly reflects the underlying microscopic structure of the nucleus. To obtain a satisfactory theoretical description of the observed structure features in the strength functions, one must base theoretical studies on a microscopic model of the nucleus in which deformation is accounted for in a consistent manner. With this aim the earlier work on β-strength functions for spherical nuclei by Hamamoto [10]), Halbleib and Sorensen [11]) and others was exended to deformed nuclei in the early 1980's by Krumlinde and Möller [12,13]) and Alkhazov *et al.* [14]). These models use a deformed single-particle model to obtain the energies and wave functions that serve as the starting point for calculating the initial state in the mother nucleus and the final state in the daughter nucleus. In this approach the important pairing and Gamow-Teller residual interactions are also taken into account. As discussed by Klapdor at this conference this deformed QRPA model developed in the early 1980's is practically identical to the approach now used by him. However, there are significant differences in how the Klapdor group and we obtain the parameters of our respective models. Whereas for the Gamow-Teller coupling constant χ we use the value $23/A$ MeV throughout the periodic system [15]), the Klapdor group [16])

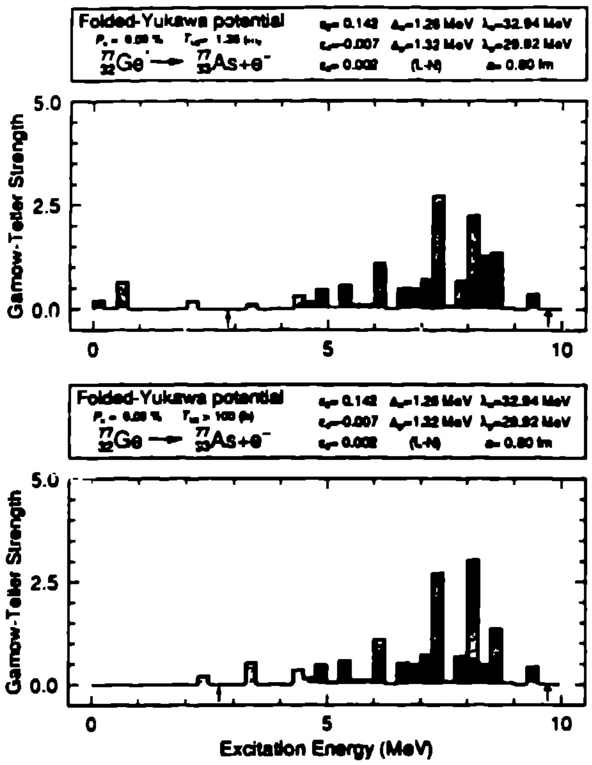

Figure 4: Illustration of different structure of Gamow-Teller β-strength function for decays from excited and ground states of ^{77}Ge.

for each individual isotope chain uses the value for which the model optimally reproduces the observed β-decay half-lives, leading to, in our opinion, an excessively large number of parameters. As examples of calculated β-strength functions and the significance of low-energy structure in these strength functions, we show in fig. 4 calculated strength functions for decay of ^{77}Ge from the ground-state configuration and from one excited configuration, with other cases shown in figs. 5 and 6. For ^{77}Ge both the $1/2^-$ ground-state decay with a half-life of 82.8 m and the $7/2^+$ isomer decay with a half-life of 48 s have been observed. The isomeric state is only a few keV above the ground state, so it is the different quantum numbers of the isomeric and ground-state configurations that so dramatically influence the decay half-lives. We see from fig. 4 that the calculated ground-state strength function corresponds to a half-life in excess of 100 h. However, just a small shift in the calculated energy of the peak just below the Q_β value would yield a half-life in agreement with experiment. The calculated strength function for decay from the isomer shows strength for decay to the ground state and nearby energies, resulting in substantially lower half-lives than occurs in decay from the parent ground state. The calculated isomer-decay half-life of 99 s is in reasonable agreement with the experimental value of 48 s.

For ^{69}Ni one has observed decay from the $9/2^+$ ground state, with a half-life of 11.2 s. With Nilsson-model wave functions, calculated results give a half-life of 18.9 s for decay from the ground state and 0.545 s from a close-lying $1/2^-$ isomeric state with energy 10

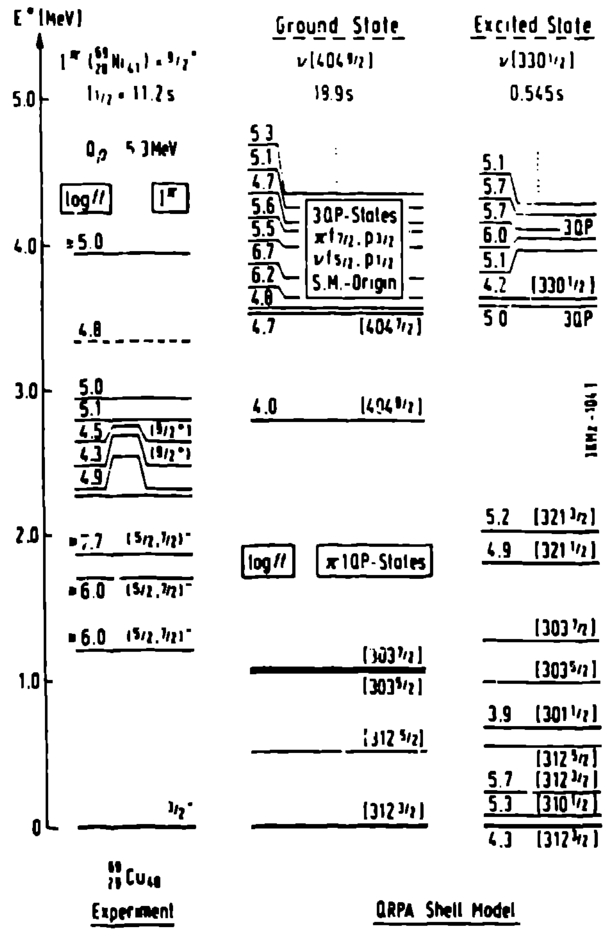

Figure 5: Experimental level scheme for ^{69}Cu with logft values for decay from the ground state of ^{69}Ni (left). A calculated decay scheme for decay from the ^{69}Ni ground state is shown in the middle. On the right we show the calculated decay scheme for decay from a low-lying $1/2^-$ excited state from which decay is allowed to the daughter ground state.

keV. In stellar environments the isomeric state would be populated to a considerable degree. In fact, at typical temperatures of 10^9 °K, the stellar half-life would be only about one tenth the terrestrial half-life. In the left-hand column of fig. 5 we show the experimentally determined level scheme for ^{69}Cu with logft values corresponding to decay from the ^{69}Ni ground state. The middle column shows a corresponding calculation for decay from the mother ground state and the right-hand column shows the calculated result for decay from the as-yet unobserved $1/2^-$ isomeric state. In the isomeric decay, beta transitions to the ^{69}Cu ground state are allowed, leading to the considerably lower half-life.

It has been observed for a considerable time that in some nuclei the magnitude of the rotational moment of inertia varies drastically between rotational bands. This feature has been interpreted as evidence for shape coexistence, corresponding to several minima in the nuclear potential-energy surface, upon which separate rotational bands

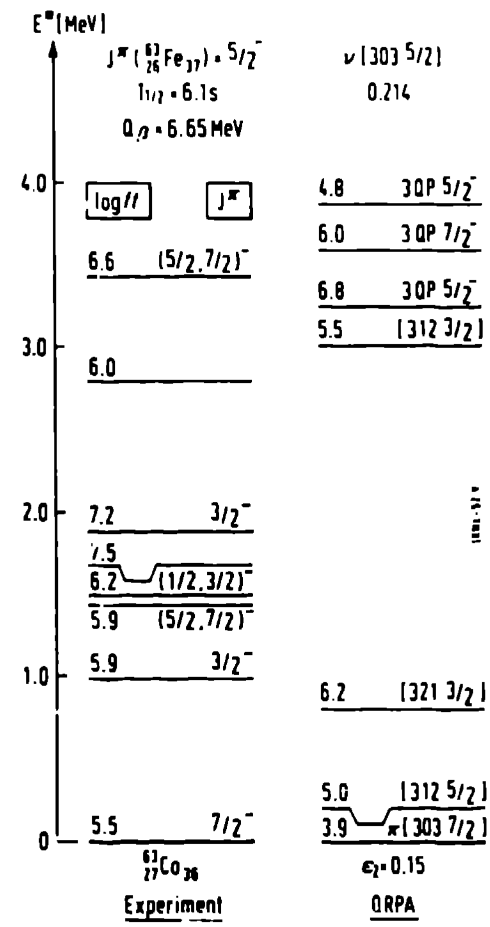

Figure 6: Experimental β-decay scheme compared to calculated strength functions for ^{63}Fe. The weak transition to the ground state and the absence of strength below 1 MeV in the experimental data indicates a low overlap between the initial $7/2^-$ state in the mother nucleus and the final daughter state. This is interpreted as evidence for shape coexistence, with decay to a *spherical* daughter ground state and *deformed* excited states.

can be built. Shape coexistence also adds complexity to the structures observed in β decay. As an example we show in fig. 6 calculated and observed level spectra and logft values for β decay from ^{63}Fe to ^{63}Co. The theoretical model, by construction, assumes identical deformations for mother and daughter nuclei. The strong, calculated ground-state to ground-state transition with a calculated logft value of 3.9 is only present as a much weaker transition in the experimental spectrum, where there is a gap of about 1 MeV between the ground state and next populated group of levels. This suggests that experimentally the ground state corresponds to a spherical configuration whereas the levels above 1 MeV correspond to levels in a deformed, secondary minimum. This interpretation is strengthened by the observation that experimentally the logft value for the ground-state transition is as low as 5.5. This low value may arise because different deformations give a low overlap between the mother and daughter $7/2^-$ wave functions.

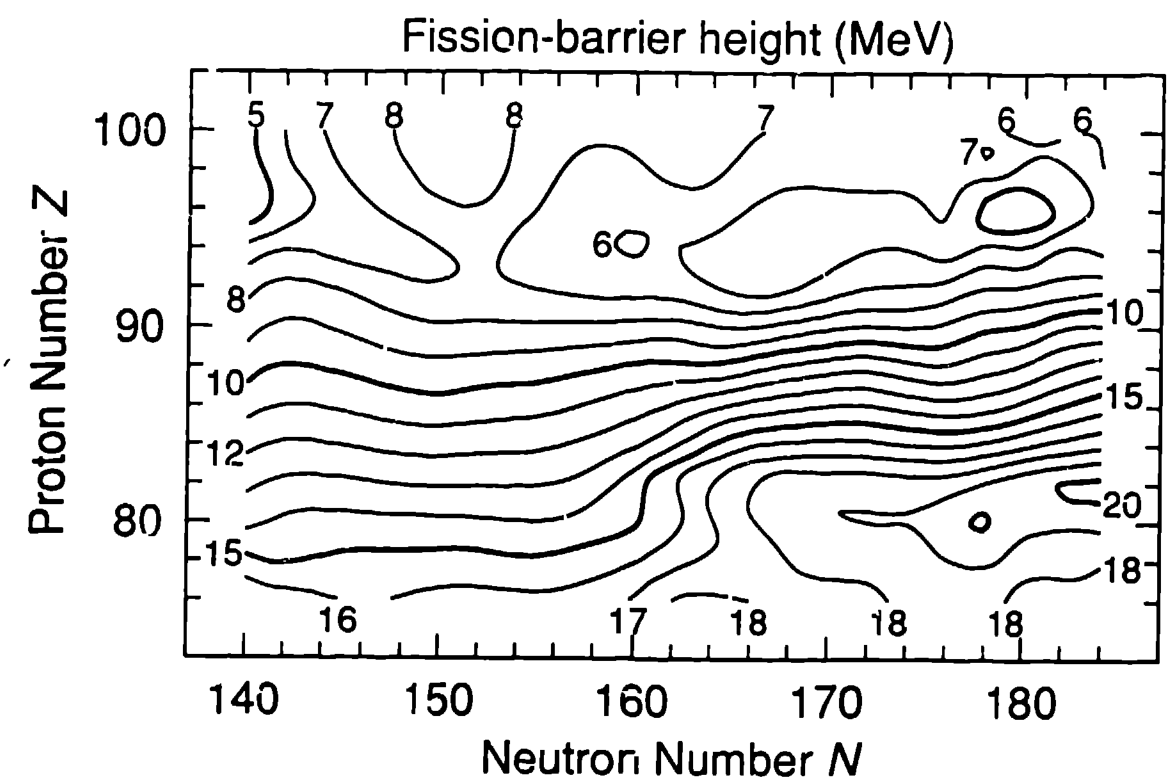

Figure 7: Calculated fission-barrier heights for even nuclei at the end of the r-process path. Relative to those in earlier calculations the barriers for neutron-rich nuclei are higher in this calculation, leading to less neutron-induced fission and less β-delayed fission.

2.4. HEAVY-ELEMENT FISSION BARRIERS

The production ratios of cosmochronometric pairs in the actinide region depend on the degree of depletion of the β-decaying A chains that occurs through fission and neutron emission during the decay back from the r-process line towards stability. It is the interplay between fission-barrier heights and structure in the β-strength functions that determines the magnitude of β-delayed fission channels. Figure 7 shows fission-barrier heights calculated in the macroscopic-microscopic model discussed in ref.[4]). The parameter space explored[17]) includes ϵ_2, ϵ_4 and ϵ_3, so that mass-asymmetric shape degrees of freedom have been included. Axially asymmetric shapes have not been taken into account in this study. They are expected to be of maximum importance in the vicinity of ^{252}Fm. Relative to those in earlier fission-barrier calculations[18]), the barriers here are several MeV higher in the neutron-rich actinide region. As a consequence, β-delayed fission is found to be of minor importance[19]).

References

1) V. M. Strutinsky, Nucl. Phys. **A95** (1967) 420.

2) V. M. Strutinsky, Nucl. Phys. **A122** (1968) 1.

3) J. R. Nix, Ann. Rev. Nucl. Sci. **22** (1972) 81.

4) P. Möller and J. R. Nix, Nucl. Phys. **A361** (1981) 117.

5) P. E. Haustein, At. Data Nucl. Data Tables **39** (1988) 185.

6) G. A. Leander and Y. S. Chen, Phys. Rev. **C37** (1988) 2744.

7) P. Armbruster, Ann. Rev. Nucl. Part. Sci. **35** (1985) 135.

8) G. Münzenberg, Rep. Prog. Phys. **51** (1988) 57.

9) K. -L. Kratz, F. -K. Thielemann, W. Hillebrandt, P. Möller, V. Harms, A. Wöhr and J. W. Truran, Proc. 6th Int. Symp. on capture gamma-ray spectroscopy, Leuven, 1987 (Inst. Phys. Conf. Ser. No. 88/J. Phys. G:Nucl. Phys. 14 Suppl., 1988) p. S331.

10) I. Hamamoto, Nucl. Phys. **62** (1965) 49.

11) J. A. Halbleib, Sr. and R. A. Sorensen, Nucl. Phys. **A98** (1967) 542.

12) J. Krumlinde, P. Möller, C. O. Wene and W. M. Howard, Proc. 4th Int. Conf. on nuclei far from stability, Helsingør, 1981 (CERN 81-09, Geneva, 1981) p. 260.

13) J. Krumlinde and P. Möller, Nucl. Phys. **A417** (1984) 419.

14) G. D. Alkhazov, A. A. Bykov, V. D. Vitman, Yu. V. Naumov, and S. Yu. Orlov, Proc. 4th Int. Conf. on nuclei far from stability, Helsingør, 1981 (CERN 81-09, Geneva, 1981) p. 238.

15) P. Möller and J. Randrup, Nucl. Phys. **A514** (1990) 1.

16) A. Staudt, E. Bender, K. Muto and H. V. Klapdor, Z. Phys. **A334** (1989) 47.

17) B. S. Meyer, P. Möller, W. M. Howard, G. J. Mathews, Proc. Conf. on 50 years with nuclear fission, Gaithersburg, 1989 (American Nuclear Society, La Grange Park, 1989) p. 587.

18) W. M. Howard and P. Möller, At. Data Nucl. Data Tables **25** (1980) 219.

19) B. S. Meyer, W. M. Howard, G. J. Mathews, K. Takahashi, P. Möller and G. A. Leander, Phys. Rev. **C39** (1989) 1876.